

1 **Estimating the sensitivity of the Priestley-Taylor coefficient to air**  
2 **temperature and humidity**

3 Ziwei Liu, Hanbo Yang \*, Changming Li, Taihua Wang

4 State Key Laboratory of Hydro-science and Engineering, Department of Hydraulic  
5 Engineering, Tsinghua University, Beijing, China

6 *Correspondence to:* Hanbo Yang (yanghanbo@tsinghua.edu.cn)

**7 Abstract**

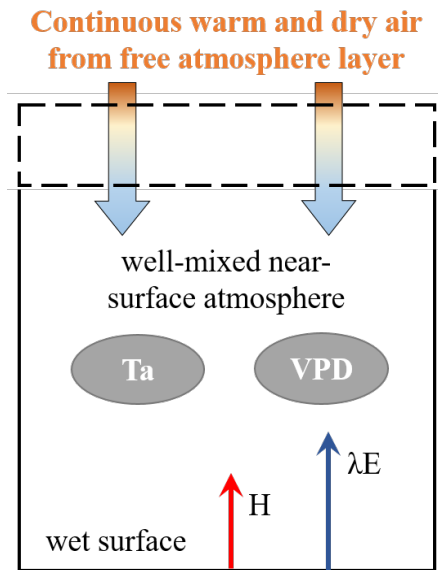
8 Priestley-Taylor (PT) coefficient ( $\alpha$ ) is generally set as a constant value or fitted as an  
9 empirical function of environmental variables, and it can bias the evaporation estimation  
10 or hydrological projections under global warming. By using an atmospheric boundary  
11 layer model, this study derives a theoretical and parameter-free equation for estimating  $\alpha$   
12 as a function of air temperature (T) and specific humidity (Q). With observations from  
13 several water bodies and non-water-limited land sites, we demonstrate that in addition to  
14 well estimating the value of  $\alpha$ , the derived expressions can also capture the sensitivity of  
15  $\alpha$  to T and Q, that is,  $d\alpha/dT$  and  $d\alpha/dQ$ .  $\alpha$  is generally negatively associated with T and Q,  
16 of which T plays a more fundamental role in controlling  $\alpha$  behaviors. Based on climate  
17 model data, we further show that this negative relationship between  $\alpha$  and T is of great  
18 importance for long-term hydrological predictions. We also provide a lookup graph for  
19 practical and broad uses to directly find the values of  $d\alpha/dT$  and  $d\alpha/dQ$  under specific  
20 conditions. Overall, the derived expression gives a physically clear and straightforward  
21 approach to quantify changes in  $\alpha$ , which is essential for PT-based hydrological  
22 simulation and projections.

23 **1. Introduction**

24 Evaporation from wet surfaces, including oceans, lakes, and reservoirs, is relevant to  
 25 global hydrological cycles and water availability. There is a long history of developing  
 26 theories and methods to estimate wet surface evaporation (Bowen, 1926; Penman, 1948;  
 27 Priestley and Taylor, 1972; Thornthwaite and Holzman, 1939; Yang and Roderick, 2019).  
 28 Among existing models, the Priestley-Taylor (PT) model/equation is known for its  
 29 transparent structure and low input requirement (Priestley and Taylor, 1972). The PT  
 30 equation is widely used in evaporation estimation across varied scales and is the basis for  
 31 various hydrologic and land surface models. Specifically, the PT equation comes from  
 32 the equilibrium evaporation ( $\lambda E_{eq}$ ), and  $\lambda E_{eq}$  can be calculated as (Slatyer and Mcilroy,  
 33 1961):

34 
$$\lambda E_{eq} = \frac{\epsilon_a}{\epsilon_a + 1} (R_n - G) \quad (1)$$

35 where  $\lambda$  (J/kg) is the latent heat of water vaporization,  $\epsilon_a = \Delta/\gamma$ ,  $\Delta$  (kPa/K) is the slope of  
 36 the saturated vapor pressure versus temperature curve (a function of temperature), and  $\gamma$   
 37 is the psychrometric constant.  $\epsilon_a$  is a function of air temperature (T).  $R_n - G$  (kPa/K) is the  
 38 available energy. The equilibrium evaporation indicates that the near-surface air is  
 39 saturated, supposing the vapor pressure deficit (VPD) is zero. However, it does not exist  
 40 in the real world (Brutsaert and Stricker, 1979; Lhomme, 1997a), due to the continuous  
 41 exchanges of warm and dry air from the entrainment layer, although water is continuously  
 42 transported from the bottom wet surface into the atmosphere through evaporation process  
 43 (Figure 1).



44  
 45 Figure 1. Atmospheric boundary layer box model describing the energy and water fluxes  
 46 at the saturated surface and atmosphere above. The dotted line represents the removable  
 47 upper boundary of the box. H and  $\lambda E$  are the sensible and latent heat fluxes. Ta is the air

48 temperature and VPD is the vapor pressure deficit.

49

50 In this case, the PT equation introduced a parameter,  $\alpha$ , known as the PT coefficient, to  
51 estimate wet surface evaporation (Priestley and Taylor, 1972).  $\alpha$  represents the effects of  
52 vertical mixing of dry and moist air and adjusts the equilibrium evaporation to the actual  
53 evaporation. So qualitatively speaking, the  $\alpha$  is impossibly lower than one because the air  
54 is always not saturated and can only infinitely close to saturated condition, no matter how  
55 moist the near-surface air is. The PT equation is:

$$56 \quad \lambda E = \alpha \frac{\epsilon_a}{\epsilon_a + 1} (R_n - G) \quad (2)$$

57 In the original study of Priestley and Taylor (1972), the value of  $\alpha$  is fitted as 1.26. While  
58 a fixed  $\alpha$  value can reasonably estimate wet surface evaporation (Yang and Roderick,  
59 2019), some studies found that  $\alpha$  varies across time and space, for example,  $\alpha$  often shows  
60 a more prominent value under cold conditions and becomes lower as warms (Xiao et al.,  
61 2020; Debruin and Keijman, 1979). This indicates that  $\alpha$  should be a variable rather than  
62 a constant (Assouline et al., 2016; Guo et al., 2015; Jury and Tanner, 1975; Lhomme,  
63 1997b; Van Heerwaarden et al., 2009; Eichinger et al., 1996; Mcnaughton and Spriggs,  
64 1986; Crago et al., 2023; Maes et al., 2019). However, the hydrology field predominantly  
65 employs the fixed value of  $\alpha = 1.26$ , despite those earlier findings being over three  
66 decades old.

67 A general method to quantify the changes in  $\alpha$  is to inverse it with observations based on  
68 Equation (2) and then build relationships among  $\alpha$  and investigated variables. Since a  
69 negative relationship between  $\alpha$  and temperature (T) is a consensus from multi-scale  
70 observations (Assouline et al., 2016; Xiao et al., 2020), many attempts empirically fitted  
71  $\alpha$  as a function of T (Andreas and Cash, 1996; Hicks and Hess, 1977; Yang and Roderick,  
72 2019). Recent work further showed that the air humidity state can also influence the  
73 spatiotemporal patterns of  $\alpha$  (Su and Singh, 2023). While those methods promote our  
74 understanding of the potential variations in  $\alpha$ , they more lie on the empirical side and pay  
75 less attention to the underlying process. Hence, various endeavors have been made to  
76 calculate  $\alpha$  through physical means, but they are often constrained by the complexity of  
77 numerous parameters. For instance, in the research conducted by Lhomme (1997b),  $\alpha$  was  
78 explicitly formulated utilizing the PM model in conjunction with boundary layer theory.  
79 Nevertheless, the formulation incorporates parameters that signify surface and  
80 aerodynamic resistances, making them hard to determine through direct measurements.  
81 Subsequently, by using a refined boundary layer model, Van Heerwaarden et al. (2009)  
82 introduced a mathematical expression for estimating  $\alpha$ , however, the expression also  
83 involves a set of parameters necessitating numerical experiments to delineate a feasible  
84 range for  $\alpha$ . Consequently, obtaining a precise  $\alpha$  estimation using conventional  
85 observations still has remained a challenge.

86 Based on a recent study by Liu and Yang (2021), here we aim to derive a physically clear,  
 87 transparent, and calibration-free equation for estimating  $\alpha$ , by introducing a governing  
 88 equation (potential vapor pressure deficit budget) into the conventional boundary layer  
 89 model. In the following sections, we will first provide the theory for estimating  $\alpha$  and its  
 90 sensitivity to climate conditions: air temperature (T) and humidity (represented by the air  
 91 specific humidity, Q). We further evaluate the theory based on measurements from the  
 92 water and non-water-limited land surfaces, followed by the influences of  $\alpha$  changes on  
 93 long-term hydrologic projections.

## 94 2. Theory

### 95 2.1 Derivation of Bowen ratio

96 Here, we use an atmospheric boundary layer-based (ABL) model as the basis for the  
 97 Bowen ratio (defined as the ratio of sensible heat fluxes to latent heat fluxes,  $H/\lambda E$ )  
 98 derivation (Liu and Yang, 2021). The fundamental conservation equations for states of  
 99 moisture and energy over the water surfaces are (Raupach, 2001):

$$100 \quad \rho c_p \frac{d\theta}{dt} = \frac{H}{h} + \frac{\rho c_p g_e}{h} (\theta_e - \theta) \quad (3)$$

$$101 \quad \rho \lambda \frac{dQ}{dt} = \frac{\lambda E}{h} + \frac{\rho \lambda g_e}{h} (Q_e - Q) \quad (4)$$

102 where  $\theta$  (K) is the potential temperature, Q is the specific humidity,  $c_p$  (J/kg/K) is the  
 103 specific heat capacity of air at constant pressure,  $g_e$  (m/s) is the entrainment flux velocity  
 104 into the ABL box, and h (m) is the height of the ABL. The subscript e indicates the  
 105 variable is evaluated at the upper boundary of the ABL (see Figure 1).

106 According to Equations (3) and (4), we can obtain a formula to calculate the rate of VPD  
 107 ( $dVPD/dt$ , see details in Liu and Yang (2021)):

$$108 \quad \frac{dVPD}{dt} = \frac{\epsilon_a H - \lambda E}{\rho \lambda h} + \frac{g_e}{h} \Delta_D \quad (5)$$

109 where  $\Delta_D$  is calculated as:

$$110 \quad \Delta_D = VPD_e - VPD \quad (6)$$

111 Under the state that air is saturated, the water vapor is continuously transported from the  
 112 water surface to the atmosphere, keeping the air saturated. In this case, there is no vertical  
 113 moisture gradient, that is, the air near the surface and the air at the upper boundary of the  
 114 ABL should be saturated, so VPD and  $VPD_e$  are both equal to zero. With Equation (6),  
 115 we can know  $\Delta_D = 0$ .

116 When air is not saturated, we can rewrite Equation (6) as:

$$117 \quad \Delta_D = Q - Q_e + [Q_{\text{sat}}(\theta_e) - Q_{\text{sat}}(\theta)] \quad (7)$$

118 where  $Q_e$  is much smaller than  $Q$ , and  $Q_{\text{sat}}(\theta_e) - Q_{\text{sat}}(\theta)$  is small (one order of magnitude  
119 smaller than  $Q$ ), so the  $\Delta_D$  roughly equals  $Q$  (Raupach, 2001; Liu and Yang, 2021).

120 Under a relatively long-term (monthly and/or longer), there is a potential VPD budget  
121 ( $d\text{VPD}/dt = 0$ ) over water surfaces (Raupach, 2001), and  $g_e$  can be estimated as the  
122 function of  $H$  and  $\lambda E$  as:

$$123 \quad g_e = \frac{H + \Lambda \cdot \lambda E}{\rho c_p \gamma_v h} \quad (8)$$

124 where  $\Lambda$  is a constant (0.07), and  $\gamma_v$  is the potential virtual temperature gradient in the  
125 free atmosphere above the ABL.  $\gamma_v h$  can be set as a fixed value of 7 K (Liu and Yang,  
126 2021). Combining with the VPD budget, Equation (5) and (8), we can obtain the  
127 expression for  $Bo$ :

$$128 \quad Bo = \begin{cases} \frac{1}{\varepsilon_a}, \text{equilibrium} \\ \frac{1 - \Lambda \chi}{\varepsilon_a + \chi}, \text{non-equilibrium} \end{cases} \quad (9)$$

129 where  $\chi = \frac{\lambda Q}{c_p \gamma_v h}$ , a function of  $Q$ .

## 130 **2.2 Theoretical formula for $\alpha$**

131 The surface energy balance is expressed as:

$$132 \quad R_n = H + \lambda E + G = (1 + Bo)\lambda E + G. \quad (10)$$

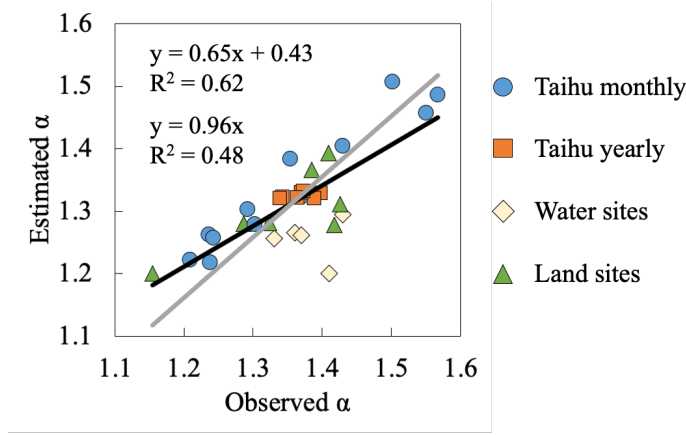
133 Combining Equations (2) and (10),  $\alpha$  can be calculated as:

$$134 \quad \alpha = \frac{1}{1 + Bo} \frac{\varepsilon_a + 1}{\varepsilon_a}. \quad (11)$$

135 With Equation (9) and (11), we can derive the formula for  $\alpha$ :

$$136 \quad \alpha = \begin{cases} 1, \text{equilibrium} \\ 1 + \frac{(\varepsilon_a \Lambda + 1)\chi}{\varepsilon_a [\varepsilon_a + 1 + (1 - \Lambda)\chi]}, \text{non-equilibrium} \end{cases} \quad (12)$$

137 Equation (12) is one of the main results in this study, and it can estimate  $\alpha$  well compared  
 138 to a large number of observations (Figure 2, please see the description of observed data  
 139 in Section 3).



140

141 Figure 2. Comparison between observed and Equation (12) calculated  $\alpha$ . The black line  
 142 is the linear fitting with intercept and the gray line is the linear fitting through origin. The  
 143 observed  $\alpha$  is inverted by the PT model.

### 144 2.3 The sensitivity of $\alpha$ to air temperature and humidity

145 According to the above derivations, we can know that  $\alpha$  is not a constant and it changes  
 146 with T and Q. The sensitivity of  $\alpha$  to T and Q,  $d\alpha/dT$  and  $d\alpha/dQ$ , determines the variation  
 147 of  $\alpha$  if the initial  $\alpha$  value is given. In this section, we derive explicit equations to estimate  
 148  $d\alpha/dT$  and  $d\alpha/dQ$ .

149 Firstly, we decompose  $\alpha$  changes in that of T and Q with partial differential equations  
 150 based on Equation (11):

$$151 \quad \frac{\partial \alpha}{\partial T} = -\frac{1}{(1 + \text{Bo}_{\text{ABL}})^2} \frac{\epsilon_a + 1}{\epsilon_a} \frac{\partial \text{Bo}_{\text{ABL}}}{\partial T} - \frac{1}{\epsilon_a^2} \frac{1}{1 + \text{Bo}_{\text{ABL}}} \frac{\partial \epsilon_a}{\partial T}, \quad (13)$$

$$152 \quad \frac{\partial \alpha}{\partial Q} = -\frac{1}{(1 + \text{Bo}_{\text{ABL}})^2} \frac{\epsilon_a + 1}{\epsilon_a} \frac{\partial \text{Bo}_{\text{ABL}}}{\partial Q}, \quad (14)$$

153 where partial differential terms of  $\frac{\partial \text{Bo}_{\text{ABL}}}{\partial T}$  and  $\frac{\partial \text{Bo}_{\text{ABL}}}{\partial Q}$  can be estimated based on

154 Equation (9) as:

$$155 \quad \frac{\partial \text{Bo}_{\text{ABL}}}{\partial T} = -\frac{1 - \Lambda \chi}{(\epsilon_a + \chi)^2} \frac{\partial \epsilon_a}{\partial T}, \quad (15)$$

$$156 \quad \frac{\partial \text{Bo}_{\text{ABL}}}{\partial Q} = -\frac{\Lambda \epsilon_a + 1}{(\epsilon_a + \chi)^2} \frac{\partial \chi}{\partial Q}. \quad (16)$$

157 where terms of  $\frac{\partial \varepsilon_a}{\partial T}$  and  $\frac{\partial \chi}{\partial Q}$  can be approximated as:

$$158 \quad \frac{\partial \varepsilon_a}{\partial T} = \frac{1}{\gamma} \frac{\partial \Delta}{\partial T}, \quad (17)$$

$$159 \quad \frac{\partial \chi}{\partial Q} = \frac{\lambda}{c_p \gamma_v h}, \quad (18)$$

160 where  $\Delta$  can be calculated as:

$$161 \quad \Delta = \frac{4098 e_s}{(T + 237.3)^2}. \quad (19)$$

162 Combining Equation (13)-(18), we can obtain:

$$163 \quad \frac{\partial \alpha}{\partial T} = \frac{1}{\gamma} \left[ \frac{1}{(1 + \text{Bo}_{\text{ABL}})^2} \frac{1 - \Lambda \chi}{(\varepsilon_a + \chi)^2} \frac{\varepsilon_a + 1}{\varepsilon_a} - \frac{1}{\varepsilon_a^2} \frac{1}{1 + \text{Bo}_{\text{ABL}}} \right] \frac{\partial \Delta}{\partial T} \quad (20)$$

$$164 \quad \frac{\partial \alpha}{\partial Q} = \frac{1}{(1 + \text{Bo}_{\text{ABL}})^2} \frac{\Lambda \varepsilon_a + 1}{(\varepsilon_a + \chi)^2} \frac{\varepsilon_a + 1}{\varepsilon_a} \frac{\lambda}{c_p \gamma_v h} \quad (21)$$

165 We can rewrite the Equation (20) as follows:

$$166 \quad \frac{\partial \alpha}{\partial T} = -\frac{1}{\gamma} \frac{\chi \left[ \varepsilon_a (\Lambda \varepsilon_a + 2) + \chi (1 - \Lambda) + 1 \right]}{(1 + \text{Bo}_{\text{ABL}})^2 (\varepsilon_a + \chi)^2 \varepsilon_a^2} \frac{\partial \Delta}{\partial T}, \quad (22)$$

167 The total differentiation of  $\alpha$  is:

$$168 \quad d\alpha = \frac{\partial \alpha}{\partial T} dT + \frac{\partial \alpha}{\partial Q} dQ, \quad (23)$$

169 thus  $\frac{d\alpha}{dT}$  and  $\frac{d\alpha}{dQ}$  can be written as:

$$170 \quad \frac{d\alpha}{dT} = \frac{\partial \alpha}{\partial T} + \frac{\partial \alpha}{\partial Q} \frac{dQ}{dT}, \quad (24)$$

$$171 \quad \frac{d\alpha}{dQ} = \frac{\partial \alpha}{\partial Q} + \frac{\partial \alpha}{\partial T} \frac{dT}{dQ}. \quad (25)$$

172 With the above equations, we can get theoretical relationships among  $\alpha$ ,  $T$ , and  $Q$ . This  
 173 derivation can provide a simple and physically clear estimation for  $\alpha$  changes. We also  
 174 obtained  $d\alpha/dT$  and  $d\alpha/dQ$  values by fitting measured data using the linear regression  
 175 model.

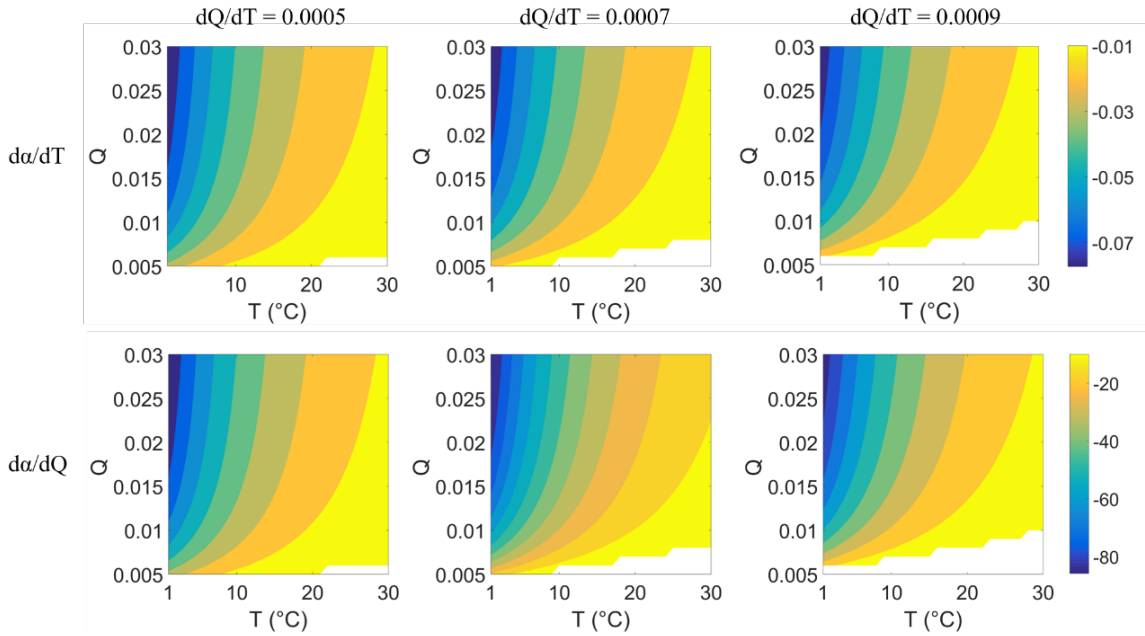
176 For practical use, we simplified the Equation (20) and (21) as:



$$177 \quad \frac{\partial \alpha}{\partial T} = -\frac{1}{\gamma} \frac{\chi}{\varepsilon_a + \chi} \frac{1}{\varepsilon_a^2} \frac{\partial \Delta}{\partial T} \quad (26)$$

$$178 \quad \frac{\partial \alpha}{\partial Q} = \frac{\varepsilon_a + 1}{\varepsilon_a (\varepsilon_a + \chi + 1)^2} \frac{\chi}{Q} \quad (27)$$

179 We further gave a numerical plot to show how  $\alpha$  changes with  $T$  and  $Q$  (Figure 3). We  
 180 plot this figure by setting a  $dQ/dT$  gradient from 0.0005, 0.0007, and 0.0009/K to ensure  
 181 cover most of the cases over water surfaces. Figure 3 can be used as the lookup graphs to  
 182 directly find  $d\alpha/dT$  and  $d\alpha/dQ$  values. For example, for a water surface with  $dQ/dT$   
 183 about 0.0007 /K, the values of  $d\alpha/dT$  and  $d\alpha/dQ$  can be found in the second column  
 184 of Figure 3.



185  
 186 Figure 3. Values of  $d\alpha/dT$  and  $d\alpha/dQ$  under different  $T$  and  $Q$ . The first and second  
 187 rows are  $d\alpha/dT$  and  $d\alpha/dQ$ , respectively. The first to third columns are under different  
 188 correlations between  $Q$  and  $T$  ( $dQ/dT$ ) as 0.0005, 0.0007, and 0.0009/K, respectively.  
 189 The blank space in each subpanel refers to values of  $d\alpha/dT$  and  $d\alpha/dQ$  are negative,  
 190 indicating situations that rarely happen in the real world (i.e., with a very high temperature,  
 191 the specific humidity is hardly deficient over wet surfaces).

### 192 3. Cases and applications

#### 193 3.1 Data

194 We select data from eddy covariance measurements on several water surfaces (Han and  
 195 Guo, 2023): (i) Lake Taihu, located in the Yangtze River Delta, China, with an area of

196 ~2,400 km<sup>2</sup>, an average depth of 1.9 m (Lee et al., 2014). There are five sites over the  
 197 Taihu surface, and the poor-quality data marked with quality flags are removed. (ii) Lake  
 198 Poyang, located in the Yangtze Plain, China, with an area of ~3,000 km<sup>2</sup> and an average  
 199 depth of 8.4 m (Zhao and Liu, 2018). (iii) Erhai, located in the Yun-Gui Plateau of China,  
 200 with an area of ~250 km<sup>2</sup> and an average depth of 10 m (Du et al., 2018). (iv) Guandu  
 201 Ponds, located in Anhui Province, China, with an area of ~0.05 km<sup>2</sup> and an average depth  
 202 of 0.8 m (Zhao et al., 2019); (v) Lake Suwa, located in Nagano, Japan, with an area of  
 203 ~13 km<sup>2</sup> and an average depth of 4 m (Taoka et al., 2020). Months with negative values  
 204 of sensible heat fluxes have not remained. Given the absence of observed heat storage (G)  
 205 at some sites, we use the sum of latent heat flux and sensible heat flux (i.e., LE+H) instead  
 206 of net radiation minus G ( $R_n-G$ ) as the measure of available energy. Using either LE+H  
 207 or  $R_n-G$  yields identical results, as our objective is to use the available energy to invert  
 208 parameter  $\alpha$  from observations. The latitude, longitude, and available data period of five  
 209 lakes/ponds are listed in Table 1. For  $\alpha$  changes in time, we use data from Lake Taihu for  
 210 investigation due to its sufficient data length. For  $\alpha$  changes in space, we calculate the  
 211 average temperature, specific humidity, and  $\alpha$  of each lake for comparison.

212 Table 1. Location and date period of each water body.

Site	Lat (°)	Lon (°)	Size (km <sup>2</sup> )	Periods <sup>a</sup>	Sample size (number of months)
Taihu	31.23	120.11	3000	2012.01 - 2018.12	341 <sup>b</sup>
Poyang	29.08	116.40	2400	2013.08 - 2017.09	41
Erhai	25.77	100.17	250	2012.01 - 2018.12	24 <sup>c</sup>
Guandu	31.97	118.25	0.05	2017.06 - 2019.12	31
Suwa	36.05	138.11	13	2016.01 - 2018.12	36

213 Note: a. Periods refer to the date of the first measurement to the date of the last one,  
 214 including months for which no data are available. b. There are five eddy covariance sites  
 215 over lake Taihu. c. Only climatology monthly data from two periods of 2012-2015 and  
 216 2015-2018 are available.

217 Observations from global flux sites (FluxNet2015 database) are also selected. We first  
 218 examine days without water stress based on the following steps (Maes et al., 2019). At  
 219 each site, the evaporative fraction (i.e., EF, latent heat flux over the sum of latent and  
 220 sensible fluxes) is first calculated, and the days with EF exceeding the 95th percentile EF  
 221 and with EF larger than 0.8 remain. Secondly, the days with soil moisture lower than 50%  
 222 of the maximum soil moisture (taken as the 98th percentile of the soil moisture series) are  
 223 removed. Days having rainfall and negative values of latent and sensible heat fluxes are  
 224 also not included. As a result, a total of ~700 non-water-stressed site-days pass the  
 225 criterion. Data is divided into seven vegetation types including croplands (CRO),  
 226 wetlands (WET), evergreen needleleaf and mixed forests (DNF\_MF), evergreen

227 broadleaf and deciduous broadleaf forests (EBF\_DBF), grasslands (GRA), close  
 228 shrublands (CSH), and woody savanna (WSA), to analyze  $\alpha$  changes in space. It should  
 229 be noted that we do not average the daily data to a monthly scale due to variations in data  
 230 sizes across different months for a specific site. Instead, we organize the selected daily  
 231 data by vegetation types, as the primary objective of utilizing land fluxes data is to assess  
 232 the derived relationship spatially rather than temporally.

233 We also collect ocean surface data from 11 CMIP6 models (under scenario SSP585, Table  
 234 2) from 2021-2100 to see the temporal changes in  $\alpha$ . The calculation is limited to the  
 235 latitudinal range 60°S to 60°N, and takes all ocean surface grids as a whole (Roderick et  
 236 al., 2014). We average the monthly data to the yearly scale and calculate  $\alpha$  every ten years  
 237 from 2021 to 2100 (i.e., 2021-2030, 2031-2040, etc.).

238 Table 2. CMIP6 models used in this study.

Model	Nation	Institute
ACCESS-ESM1-5	Australia	CSIRO
CanESM5	Canada	CCCma
CESM2-WACCM	USA	NCAR
CMCC-CM2-SR5	Italy	CMCC
CMCC-ESM2	Italy	CMCC
FGOALS-g3	China	CAS
FIO-ESM-2-0	China	CAS
MPI-ESM1-2-HR	Germany	MPI-M
MPI-ESM1-2-LR	Germany	MPI-M
NorESM2-LM	Norway	NCC
NorESM2-MM	Norway	NCC

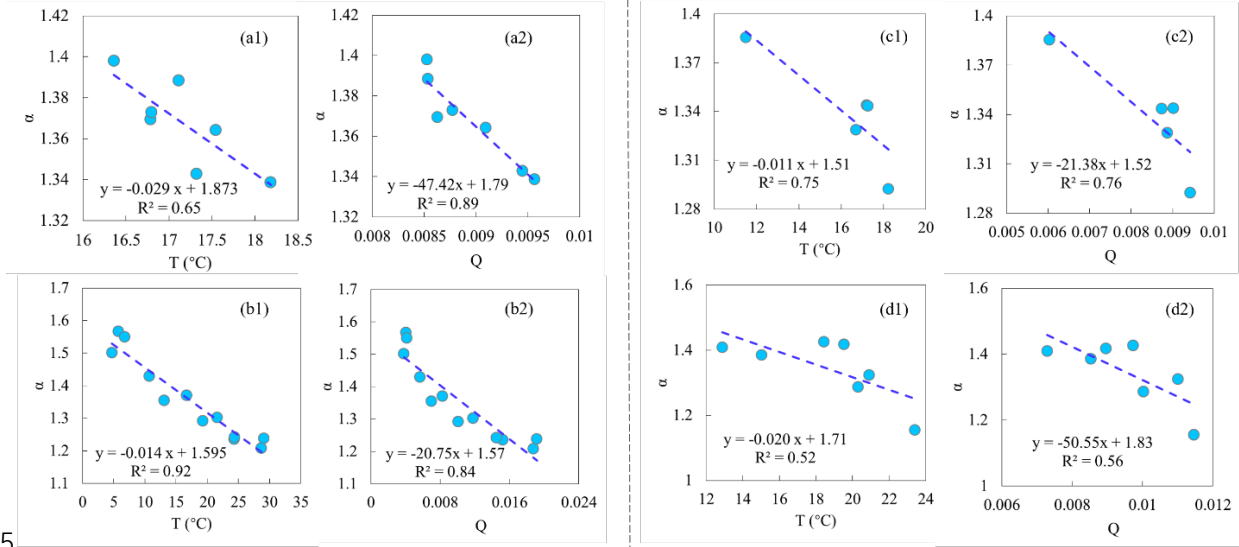
239 Note: CSIRO: Commonwealth Scientific and Industrial Research Organization;  
 240 CCCma: Canadian Centre for Climate Modelling and Analysis; NCAR: National Center  
 241 for Atmospheric Research; CMCC: Euro-Mediterranean Center on Climate Change;  
 242 CAS: Chinese Academy of Sciences; MPI-M: Max Planck Institute for Meteorology;  
 243 NCC: Norwegian Climate Centre.

## 244 3.2 Results

### 245 (1) Temporal and spatial changes in $\alpha$

246 We used yearly and climatology monthly (from Jan to Dec) data from Lake Taihu to  
 247 investigate the temporal variation in  $\alpha$ .  $\alpha$  is firstly inversed by the PT model and  
 248 measurements, and then we found significant negative relationships of  $\alpha$  with both T and  
 249 Q (Figure 4). On the yearly scale, the regressed values of  $d\alpha/dT$  and  $d\alpha/dQ$  are -  
 250 0.029/°C and -47.42, and the values on the seasonal scale are -0.014/°C and -20.75,  
 251 respectively.  $d\alpha/dT$  on the seasonal scale is higher than that on the yearly scale because

252 the variation range of  $\alpha$  on the seasonal scale is more extensive. Theoretical derived  $d\alpha/dT$   
 253 and  $d\alpha/dQ$  roughly match with the regressed values (Table 3). We also analyzed on the  
 254 ten-day scale and obtained robust results (see Appendix Figure A1 and Table A1).



255 Figure 4. Temporal and spatial relationships of  $\alpha$  and temperature (T) and specific  
 256 humidity (Q). (a-b) Temporal relationships based on lake Taihu data: (a) yearly data, and  
 257 (b) climatology monthly data. (c-d) Spatial relationships: (c) data from five water surface  
 258 sites, and (d) land surface data from FluxNet2015, each circle representing one vegetation  
 259 type. The linear regression line and correlation coefficient ( $R^2$ ) are shown in each  
 260 subpanel.  
 261

262  
 263 Table 3 Sensitivity of  $\alpha$  to temperature (T) and specific humidity (Q) by regression and  
 264 theoretical derivation.

		$d\alpha/dT$ ( $^{\circ}C$ )		$d\alpha/dQ$	
		regression	derivation	regression	derivation
Temporal	yearly	-0.029	-0.023	-47.42	-37.95
	seasonally	-0.014	-0.011	-20.75	-18.38
Spatial	water sites	-0.011	-0.012	-21.38	-24.30
	land sites	-0.020	-0.016	-50.55	-40.47

265  
 266 Spatial relationships of  $\alpha$  with T and Q are similar to that in time, i.e., higher T and Q  
 267 generally correspond to lower  $\alpha$ , supported by measurements over both water and land  
 268 surfaces (Figure 4). For the water surfaces, the values of  $d\alpha/dT$  and  $d\alpha/dQ$  are -  
 269  $0.011/^{\circ}C$  and  $-21.38$ , and the values for land surfaces are  $-0.020/^{\circ}C$  and  $-50.55$ . The  
 270 derived  $d\alpha/dT$  and  $d\alpha/dQ$  reasonably match well with the regressed values (Table 3).  
 271 The correlations (represented by  $R^2$  in Figure 4) between  $\alpha$  and T,  $\alpha$  and Q of water  
 272 surfaces are higher than those over the land surfaces. This indicates that changes in  $\alpha$  are  
 273 more associated with T and Q over water surfaces, which may be because T and Q  
 274 dominate the water surface evaporation process, while some other factors, like vegetation

275 and wind speed, also play specific roles over land surfaces.

276 Based on Equation (20) to (22),  $\partial\alpha/\partial T$  is always a negative value, and  $\partial\alpha/\partial Q$  is  
 277 always positive. The regressed and derived  $d\alpha/dT$  and  $d\alpha/dQ$  are both negative.  
 278 Combined with Equations (24), (25) and the positive relationship between T and Q, the  
 279  $\partial\alpha/\partial T$  plays a more critical role in determining (the signs of)  $d\alpha/dT$  and  $d\alpha/dQ$ , that  
 280 is,  $|\partial\alpha/\partial T| > \partial\alpha/\partial Q \cdot dQ/dT$  and  $|\partial\alpha/\partial T \cdot dT/dQ| > \partial\alpha/\partial Q$ . Specifically, based on the data  
 281 from lake Taihu (for detecting  $\alpha$  changes in time) and data from different water surface  
 282 sites and land surface sites (for detecting  $\alpha$  changes in space), we found the contribution  
 283 of  $\partial\alpha/\partial T \cdot dT$  to  $d\alpha$  is  $\sim 70\%$ , much more significant than that of  $\partial\alpha/\partial Q \cdot dQ$  of  $\sim 30\%$   
 284 (Table 4). Therefore, according to the evaporation process over the wet surface (Section  
 285 2.1) and the above analyses, we can conclude that  $\alpha$  is fundamentally controlled by T and  
 286 modulated by Q.

287 Table 4. Contributions of changes in temperature (T) and specific humidity (Q) to  
 288 changes in  $\alpha$ .

		$d\alpha$	contribution of $\frac{\partial\alpha}{\partial T}dT$	contribution of $\frac{\partial\alpha}{\partial Q}dQ$
Temporal	yearly	-0.035	78%	22%
	seasonally	-0.256	67%	33%
Spatial	water sites	-0.081	68%	32%
	land sites	-0.167	77%	23%
Average		----	72.5%	27.5%

289 Note: Since  $d\alpha = \frac{\partial\alpha}{\partial T}dT + \frac{\partial\alpha}{\partial Q}dQ$ , the contribution of  $\frac{\partial\alpha}{\partial T}dT$  is calculated as

290  $\left| \frac{\partial\alpha}{\partial T}dT \right| / \left| \frac{\partial\alpha}{\partial T}dT + \frac{\partial\alpha}{\partial Q}dQ \right|$ , and is the contribution of  $\frac{\partial\alpha}{\partial Q}dQ$  calculated as

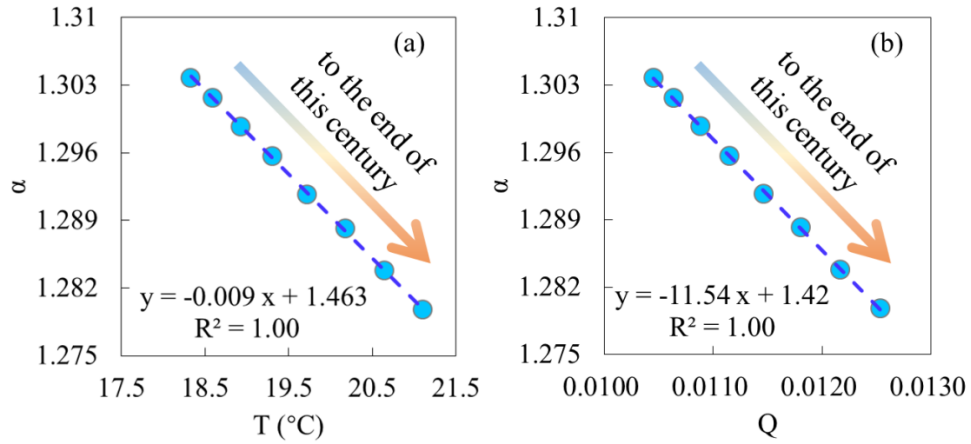
291  $\left| \frac{\partial\alpha}{\partial Q}dQ \right| / \left| \frac{\partial\alpha}{\partial T}dT + \frac{\partial\alpha}{\partial Q}dQ \right|$ .  $d\alpha$  refers to the estimated variation of  $\alpha$  from lowest to highest

292 T (also from lowest to highest Q since T and Q are positively correlated).

293 Derived  $d\alpha/dT$  and  $d\alpha/dQ$  have more or less errors compared to the regressed values.  
 294 Several reasons can explain this: (i) errors in measurements of eddy covariance systems;  
 295 (ii) the additional factors other than T and Q, like wind speed, can also influence  $\alpha$ ; (iii)  
 296 the relationship of  $\alpha$  and T (also  $\alpha$  and Q) cannot be well represented by the linear  
 297 regression model. Besides, the water surface size effects on evaporation and  $\alpha$ , reported  
 298 by Han and Guo (2023), are not well considered in the presented derivation. Nevertheless,  
 299 the derived expression can fairly match the observations of water bodies with various  
 300 sizes (Table 3).

301 **(2) Potential applications for global projections**

302 Based on CMIP6 ocean surface data, we also detected significant negative relationships  
 303 of  $\alpha$  with T and Q (Figure 5).  $d\alpha/dT$  and  $d\alpha/dQ$  obtained by the linear regression are -  
 304 0.009/°C and -11.54, respectively. The derived  $d\alpha/dT$  and  $d\alpha/dQ$  are close to the  
 305 regressed value as -0.009/°C and -10.74. We further compared the changes in T, Q, and  
 306 heat fluxes between the first and the last ten years in 2021-2100 (Table 5). To the end of  
 307 this century, CMIP6 models predict that ocean average available energy ( $R_n-G$ ) and latent  
 308 heat flux (also evaporation) will increase by  $\sim 3.1$  W/m<sup>2</sup> and  $\sim 6.0$  W/m<sup>2</sup>, respectively.  
 309 Using the PT model with the fixed  $\alpha$  (1.26), predicted evaporation shows an increase of  
 310  $\sim 8.0$  W/m<sup>2</sup>, far higher than climate models' direct output (with a relative bias of  $\sim 30\%$ ).  
 311 Based on derived  $\alpha$ , ocean evaporation shows a much smaller increase of  $\sim 5.8$  W/m<sup>2</sup>, with  
 312 less than 5% relative bias compared to CMIP6 values (Figure 6). This indicates that  
 313 changes in  $\alpha$  should be well considered for the long-term projections. So here we suggest  
 314 introducing the negative relationship between  $\alpha$  and T, proposed in this study, into the  
 315 original PT model to correct for the overestimated sensitivity of evaporation to  
 316 temperature (Liu et al., 2022), which could also improve the reliability of global long-  
 317 term drought predictions (Greve et al., 2019).



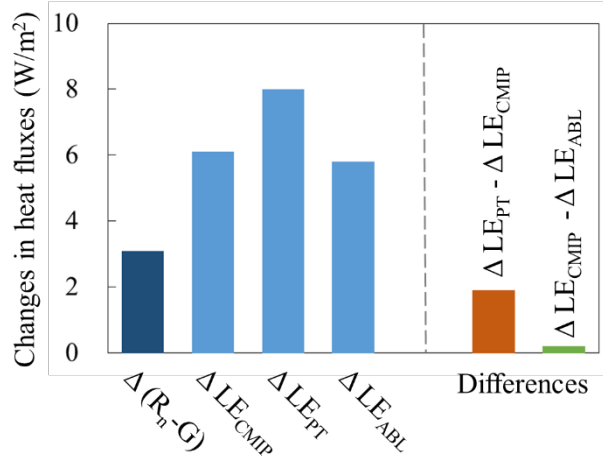
318  
 319 Figure 5. Temporal relationship of (a)  $\alpha$  and temperature (T), and (b)  $\alpha$  and specific  
 320 humidity (Q) over global ocean surfaces. Each dot denotes the data in each 10-year  
 321 window (2021-2030, 2031-2041, ..., 2091-2100), from left to right is from 2021-2030 to  
 322 2091-2100.

323  
 324 Table 5. Ocean surface temperature, specific humidity, and heat fluxes at the first ten  
 325 years (2021-2030) and the end of the 21<sup>st</sup> century (2091-2100). T, Q,  $R_n-G$ , and LE are  
 326 direct outputs of climate models.  $\alpha$ -CMIP refers to  $\alpha$  inversed by the PT model with CMIP  
 327 data.  $LE_{PT}$  is calculated by the PT model with fixed  $\alpha$  at 1.26.  $\alpha$ -ABL refers to  $\alpha$  estimated  
 328 by the ABL model.  $LE_{ABL}$  is calculated by the PT model with  $\alpha$ -ABL.

Period	T	Q	$R_n-G$	LE	$\alpha$ -CMIP	$LE_{PT}$	$\alpha$ -ABL	$LE_{ABL}$
	(°C)	(-)	(W/m <sup>2</sup> )	(W/m <sup>2</sup> )		(W/m <sup>2</sup> )		(W/m <sup>2</sup> )

2021-2030	18.1	0.010	122.9	106.8	1.304	103.2	1.316	107.7
2091-2100	21.1	0.013	126.0	112.9	1.279	111.2	1.287	113.5
$\Delta$	3.0	0.003	3.1	6.1	-0.025	8.0	-0.029	5.8

329



330

331 Figure 6. Stylized diagram showing the average changes in heat fluxes over global  
332 ocean surfaces.

#### 333 4. Discussions and Conclusions

334 In this study, we employed an open boundary layer model with a governing potential VPD  
335 budget (Raupach, 2001, 2000), originally integrated by Liu and Yang (2021), to formulate  
336 an expression for the Priestley-Taylor coefficient,  $\alpha$ . Notably, the governing equation  
337 allows the derived expression has no calibrated parameters and can estimate a precise  $\alpha$   
338 value with normal observations, rendering it superior to other methods that also built with  
339 the boundary layer theory (Lhomme, 1997b; Van Heerwaarden et al., 2009). With the  
340 expression and a variety of measurements, we further demonstrated that temperature  
341 exerts a more significant influence on variations in  $\alpha$ , as opposed to specific humidity. We  
342 suggest that for studies focusing on evaporation and/or drought projections, it is crucial  
343 to thoroughly characterize the negative correlation between  $\alpha$  and temperature, a  
344 relationship easily determined using the derived expression.

345 It should be noted that except for the PT model, the PM-based model can be also used to  
346 estimate wet surface evaporation (Penman, 1948; Shuttleworth, 1993). While PM-based  
347 equations encapsulate all processes that possibly affect evaporation, the PT model, taking  
348 evaporation as a simple function of radiation and temperature, takes more account of the  
349 feedback/balance between the surface and near atmosphere (Figure 1). Besides, it has  
350 been noted that the PM-based models may fail at certain limits, and cannot capture the  
351 sensitivity of evaporation to temperature changes (Liu et al., 2022; McColl, 2020). So in  
352 this case, also with the fact that the PT model is currently one of the most popular

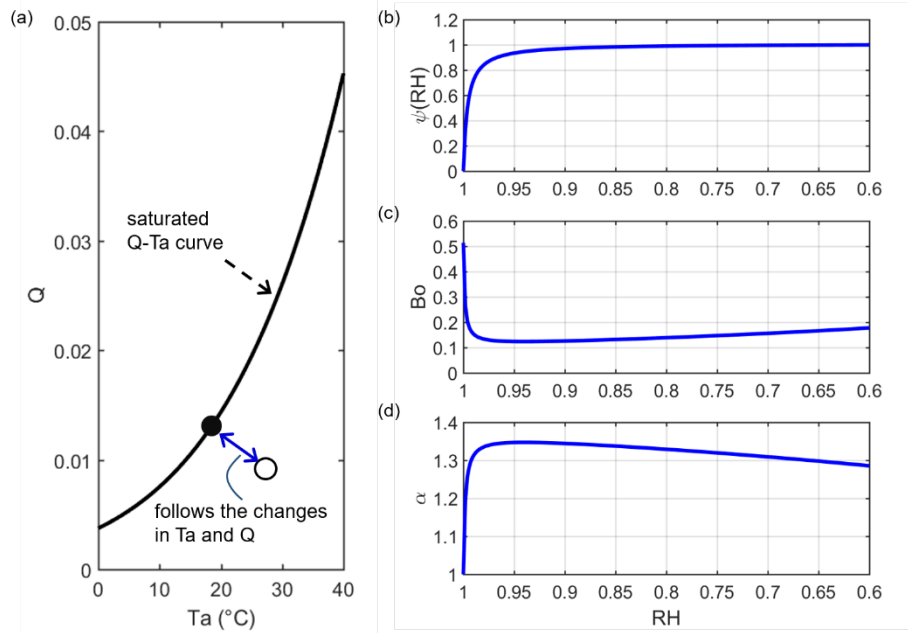
353 equations due to its low input requirements, revisiting this classic model can greatly  
 354 promote its adaption under the changing climate. Meanwhile, some revised PT equations  
 355 can also be used to estimate the parameter  $\alpha$  (Yang and Roderick, 2019; De Bruin and  
 356 Holtslag, 1982). However, these modifications often exhibit significant deviations  
 357 (Figure A2). Specifically, the model developed by De Bruin and Holtslag (1982) is based  
 358 on data from one specific site in the Netherlands, and the model built by Yang and  
 359 Roderick (2019) comes from the fitness of global ocean surface data. These equations are  
 360 primarily calibrated to match observed evaporation rates, while the underlying process is  
 361 generally overlooked.

362 In Section 2.1, it was suggested that  $\Delta_D = 0$  for the saturated air while  $\Delta_D \approx Q$  for the  
 363 non-saturated air. In theory, it is expected that the transition track between saturated and  
 364 non-saturated states should be continuous and smooth. That is, the changes in the value  
 365 of  $\Delta_D$  between the saturated (0) and non-saturated (Q) states should follow the  
 366 variations in air energy and moisture (Figure 7). Since the relative humidity (RH) includes  
 367 both information on air temperature and humidity, here we introduce a possible track of  
 368  $\Delta_D$  depending on RH as:  $\Delta_D = \psi(\text{RH}) \cdot Q$ . As we expect, the value of  $\Delta_D$  approaches 0  
 369 when the air is very moist (i.e., very close to the saturated state and RH close to 1), so  $\psi$   
 370 should be a nonlinear and monotone convex function of RH. We give a possible  
 371 expression of  $\psi(\text{RH})$  as:

$$372 \quad \psi(\text{RH}) = 1 - \frac{1}{1 + m \times \left( \frac{\text{RH}_{\max} - \text{RH}}{\text{RH} - \text{RH}_{\min}} \right)^n} \quad (28)$$

373 where  $\text{RH}_{\max}$  is 1, and  $\text{RH}_{\min}$  is 0.6 (Mccoll and Tang, 2023) over the water surfaces.  $m$   
 374 and  $n$  are shape parameters. To make  $\psi(\text{RH})$  simple, we fixed  $n$  at 1, and let  $m$  be 100.  
 375 The relationship between  $\psi(\text{RH})$  and RH can be viewed in Figure 7 (b). For a specific  
 376 case that  $T$  at 18 °C, we show the changes in  $\text{Bo}$  and  $\alpha$  with RH in Figure 7 (c)-(d).  
 377 Although there is a dramatic shift in  $\text{Bo}$  or  $\alpha$ , it appears when RH is at 0.95-1, which is  
 378 outside the vast majority of actual cases (RH is generally smaller than 0.9 on a monthly  
 379 or longer scale). After the shift point, with RH decreases,  $\psi(\text{RH})$ ,  $\text{Bo}$ , and  $\alpha$  remain  
 380 roughly stable. It is worth noting that Equation (28) (with specific parameters) is one  
 381 possible case that connects the transition between saturated and non-saturated air states,  
 382 a fine determination may be affected by local conditions, but  $\Delta_D$  value around  $Q$  is  
 383 expected for most of the cases.





384

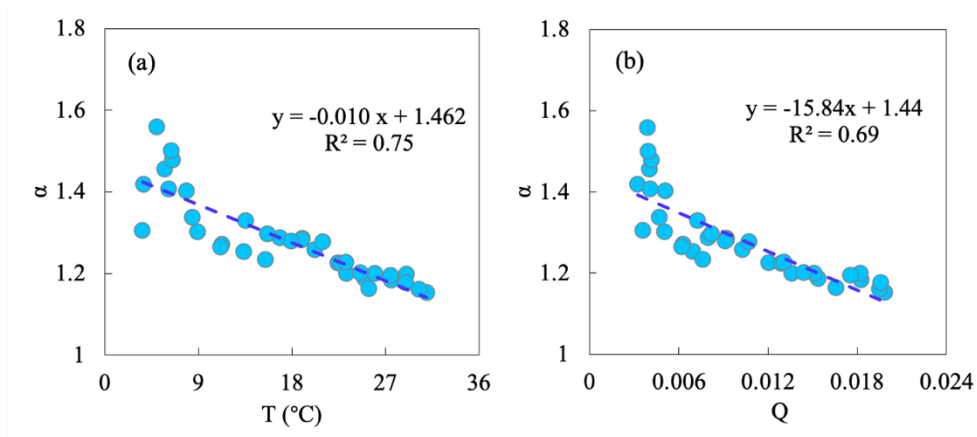
385 Figure 7. (a) Transition between saturated and non-saturated air states. The filled circle  
 386 represents one case in which the air is saturated (saturated state) and the open circle  
 387 represents one case in which air is not saturated (non-saturated state). (b) Relationship  
 388 between  $\psi(\text{RH})$  and  $\text{RH}$  with Equation (28). (c)-(d) Changes in  $B_0$  and  $\alpha$  as the  
 389 function of  $\text{RH}$  when air temperature is fixed at  $18^{\circ}\text{C}$ .

390 We recommend utilizing the derived model under warm conditions, for example, when  
 391 the air temperature exceeds zero, to account for the prerequisite of a well-mixed boundary  
 392 layer. In extremely cold regions or seasons, the water surface temperature can be lower  
 393 than the air temperature, resulting in a downward sensible heat flux (De Bruin, 1982).  
 394 Under such circumstances, the boundary layers exhibit relative stability and may not  
 395 reach a well-mixed state. Additionally, we advise adopting a temporal scale ranging from  
 396 weekly to monthly when applying the derived model. This is because the potential VPD  
 397 budget (the governing equation) may not be rapidly achieved, such as on a diurnal or daily  
 398 basis. Furthermore, over a longer term, the sensible heat flux typically manifests as  
 399 upward in the majority of scenarios than on a fine temporal scale.

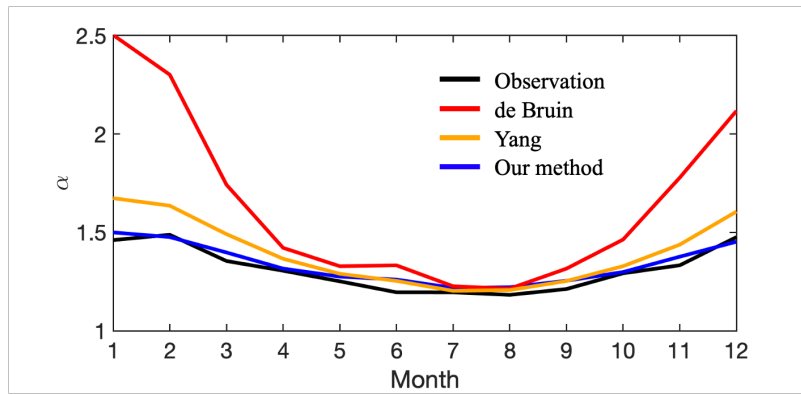
400 The derived formula for  $\alpha$  has important practical meanings. For example, it would be  
 401 useful for estimating water surface evaporation and actual evapotranspiration based on  
 402 the PT model (Miralles et al., 2011; Maes et al., 2019). It can also help to constrain the  
 403 relationships among  $\alpha$ ,  $T$ , and  $Q$  in the complementary relationship, whose performance  
 404 previously depended on the inversed  $\alpha$  (Liu et al., 2016). Besides, considering the impacts  
 405 of changing climate on  $\alpha$  can significantly improve the performance of the hydrologic  
 406 model in runoff simulations and predictions (Pimentel et al., 2023).

407

408 **Appendix A.**



409  
 410 Figure A1. Relationships of  $\alpha$  with (a) temperature (T) and with (b) specific humidity (Q)  
 411 on the ten-day scale using water surface observations collected over Lake Taihu.  
 412



413  
 414 Figure A2. Observed (black) and estimated  $\alpha$  over lake Taihu. The blue line is  $\alpha$   
 415 estimated with our method, and the red and orange lines are with two revised PT  
 416 equations. The red line represents  $\alpha=1+\frac{20}{\frac{\Delta}{\Delta+\gamma}(R_n-G)}$  (De Bruin and Holtslag, 1982), and  
 417 the orange line represents  $\alpha=\frac{\Delta+\gamma}{\Delta+0.24\gamma}$  (Yang and Roderick, 2019).

418  
 419 Table A1. Sensitivity of  $\alpha$  to temperature (T) and specific humidity (Q) on the ten-day  
 420 scale.

$d\alpha/dT$ ( $^{\circ}\text{C}$ )		$d\alpha/dQ$	
regression	derivation	regression	derivation
-0.010	-0.011	-15.84	-18.12

421

422 **Author Contributions**

423 Conceptualization: Ziwei Liu, Hanbo Yang. Data curation: Ziwei Liu. Formal analysis:  
424 Ziwei Liu. Funding acquisition: Hanbo Yang. Methodology: Ziwei Liu, Hanbo Yang.  
425 Software: Ziwei Liu. Supervision: Hanbo Yang. Writing – original draft: Ziwei Liu.  
426 Writing – review & editing: Changming Li, Taihua Wang, Hanbo Yang.

427 **Data availability**

428 Data of Lake Taihu can be obtained from Harvard Dataverse,  
429 <https://doi.org/10.7910/DVN/HEWCWM>. The data of Poyang Lake can be obtained  
430 from Zhao and Liu (2018) and Gan and Liu (2020). The data of Erhai can be obtained  
431 from Du et al. (2018). The data of Guandu can be obtained from Zhao et al. (2019). The  
432 data of Suwa lake can be obtained from the AsiaFlux  
433 ([http://asiaflux.net/index.php?page\\_id=1355](http://asiaflux.net/index.php?page_id=1355)). FluxNet 2015 data are available at  
434 <https://fluxnet.fluxdata.org/data/download-data/>. CMIP6 data can be obtained from  
435 Earth System Grid Federation (<https://esgf-node.llnl.gov>).

436 **Acknowledgments**

437 This study is financially supported by the National Natural Science Foundation of China  
438 (grant nos. 51979140, 42041004).

439 **Competing interests**

440 There are no competing interests.

441 **References:**

- 442 Andreas, E. L. and Cash, B. A.: A new formulation for the Bowen ratio over saturated surfaces, *Journal of*  
443 *Applied Meteorology*, 35, 1279-1289, 10.1175/1520-0450(1996)035<1279:anfftb>2.0.co;2, 1996.
- 444 Assouline, S., Li, D., Tyler, S., Tanny, J., Cohen, S., Bou-Zeid, E., Parlange, M., and Katul, G. G.: On the  
445 variability of the Priestley-Taylor coefficient over water bodies, *Water Resources Research*, 52, 150-163,  
446 10.1002/2015wr017504, 2016.
- 447 Bowen, I. S.: The ratio of heat losses by conduction and by evaporation from any water surface, *Physical*  
448 *Review*, 27, 779-787, 10.1103/PhysRev.27.779, 1926.
- 449 Brutsaert, W. and Stricker, H. J. W. r. r.: An advection-aridity approach to estimate actual regional  
450 evapotranspiration, 15, 443-450, 1979.
- 451 Crago, R. D., Szilagyi, J., and Qualls, R. J.: What is the Priestley–Taylor wet-surface evaporation parameter?  
452 Testing four hypotheses, *Hydrol. Earth Syst. Sci.*, 27, 3205-3220, 10.5194/hess-27-3205-2023, 2023.
- 453 De Bruin, H. and Holtslag, A.: A simple parameterization of the surface fluxes of sensible and latent heat  
454 during daytime compared with the Penman-Monteith concept, *Journal of Applied Meteorology and*  
455 *Climatology*, 21, 1610-1621, 1982.
- 456 de Bruin, H. A. R.: Temperature and energy balance of a water reservoir determined from standard weather  
457 data of a land station, *Journal of Hydrology*, 59, 261-274, [https://doi.org/10.1016/0022-1694\(82\)90091-9](https://doi.org/10.1016/0022-1694(82)90091-9),  
458 1982.
- 459 Debruin, H. A. R. and Keijman, J. Q.: Priestley-taylor evaporation model applied to a large, shallow lake  
460 in the netherlands, *Journal of Applied Meteorology*, 18, 898-903, 10.1175/1520-  
461 0450(1979)018<0898:tptema>2.0.co;2, 1979.
- 462 Du, Q., Liu, H. Z., Liu, Y., Wang, L., Xu, L. J., Sun, J. H., and Xu, A. L.: Factors controlling evaporation  
463 and the CO<sub>2</sub> flux over an open water lake in southwest of China on multiple temporal scales, *International*  
464 *Journal of Climatology*, 38, 4723-4739, 10.1002/joc.5692, 2018.
- 465 Eichinger, W. E., Parlange, M. B., and Stricker, H.: On the concept of equilibrium evaporation and the value  
466 of the Priestley-Taylor coefficient, *Water Resources Research*, 32, 161-164, 1996.
- 467 Gan, G. and Liu, Y.: Heat Storage Effect on Evaporation Estimates of China's Largest Freshwater Lake,  
468 125, e2019JD032334, <https://doi.org/10.1029/2019JD032334>, 2020.
- 469 Greve, P., Roderick, M. L., Ukkola, A. M., and Wada, Y.: The aridity Index under global warming,  
470 *Environmental Research Letters*, 14, 10.1088/1748-9326/ab5046, 2019.
- 471 Guo, X., Liu, H., and Yang, K. J. B.-L. M.: On the application of the Priestley–Taylor relation on sub-daily  
472 time scales, 156, 489-499, 2015.
- 473 Han, S. and Guo, F.: Evaporation From Six Water Bodies of Various Sizes in East Asia: An Analysis on  
474 Size Dependency, *Water Resources Research*, 59, 10.1029/2022wr032650, 2023.
- 475 Hicks, B. B. and Hess, G. D.: On the Bowen Ratio and Surface Temperature at Sea, *Journal of Physical*  
476 *Oceanography*, 7, 141-145, 10.1175/1520-0485(1977)007<0141:otbras>2.0.co;2, 1977.
- 477 Jury, W. and Tanner, C. J. A. J.: Advection Modification of the Priestley and Taylor Evapotranspiration  
478 Formula 1, 67, 840-842, 1975.
- 479 Lee, X., Liu, S., Xiao, W., Wang, W., Gao, Z., Cao, C., Hu, C., Hu, Z., Shen, S., Wang, Y., Wen, X., Xiao,  
480 Q., Xu, J., Yang, J., and Zhang, M.: THE TAIHU EDDY FLUX NETWORK An Observational Program on  
481 Energy, Water, and Greenhouse Gas Fluxes of a Large Freshwater Lake, *Bulletin of the American*  
482 *Meteorological Society*, 95, 1583-1594, 10.1175/bams-d-13-00136.1, 2014.

- 483 Lhomme, J. P.: An examination of the Priestley-Taylor equation using a convective boundary layer model,  
484 *Water Resources Research*, 33, 2571-2578, 1997a.
- 485 Lhomme, J. P.: A theoretical basis for the Priestley-Taylor coefficient, *Boundary-Layer Meteorology*, 82,  
486 179-191, 1997b.
- 487 Liu, X., Liu, C., and Brutsaert, W.: Regional evaporation estimates in the eastern monsoon region of China:  
488 Assessment of a nonlinear formulation of the complementary principle, 52, 9511-9521,  
489 <https://doi.org/10.1002/2016WR019340>, 2016.
- 490 Liu, Z. and Yang, H.: Estimation of Water Surface Energy Partitioning With a Conceptual Atmospheric  
491 Boundary Layer Model, *Geophysical Research Letters*, 48, e2021GL092643,  
492 <https://doi.org/10.1029/2021GL092643>, 2021.
- 493 Liu, Z., Han, J., and Yang, H.: Assessing the ability of potential evaporation models to capture the sensitivity  
494 to temperature, *Agricultural and Forest Meteorology*, 317, 108886, 2022.
- 495 Maes, W. H., Gentine, P., Verhoest, N. E. C., and Miralles, D. G.: Potential evaporation at eddy-covariance  
496 sites across the globe, *Hydrology and Earth System Sciences*, 23, 925-948, 10.5194/hess-23-925-2019,  
497 2019.
- 498 McColl, K. A. and Tang, L. I.: An analytic theory of near-surface relative humidity over land, *Journal of*  
499 *Climate*, <https://doi.org/10.1175/JCLI-D-23-0342.1>, 2023.
- 500 McNaughton, K. and Spriggs, T.: A MIXED-LAYER MODEL FOR REGIONAL EVAPORATION,  
501 *Boundary-Layer Meteorology*, 34, 243-262, 10.1007/bf00122381, 1986.
- 502 Miralles, D. G., Holmes, T., De Jeu, R., Gash, J., Meesters, A., Dolman, A. J. H., and Sciences, E. S.: Global  
503 land-surface evaporation estimated from satellite-based observations, 15, 453-469, 2011.
- 504 Penman, H. L.: Natural evaporation from open water, bare soil and grass, *Proceedings of the Royal Society*  
505 *of London Series a-Mathematical and Physical Sciences*, 193, 120-145, 10.1098/rspa.1948.0037, 1948.
- 506 Pimentel, R., Arheimer, B., Crochemore, L., Andersson, J. C. M., Pechlivanidis, I. G., and Gustafsson, D.:  
507 Which Potential Evapotranspiration Formula to Use in Hydrological Modeling World-Wide?, 59,  
508 e2022WR033447, <https://doi.org/10.1029/2022WR033447>, 2023.
- 509 Priestley, C. H. B. and Taylor, R. J.: Assessment of surface heat-flux and evaporation using large-scale  
510 parameters, *Monthly Weather Review*, 100, 81-92, 10.1175/1520-0493(1972)100<0081:otaosh>2.3.co;2,  
511 1972.
- 512 Raupach, M. R.: Equilibrium evaporation and the convective boundary layer, *Boundary-Layer Meteorology*,  
513 96, 107-141, 10.1023/a:1002675729075, 2000.
- 514 Raupach, M. R.: Combination theory and equilibrium evaporation, *Quarterly Journal of the Royal*  
515 *Meteorological Society*, 127, 1149-1181, 10.1002/qj.49712757402, 2001.
- 516 Roderick, M. L., Sun, F., Lim, W. H., and Farquhar, G. D.: A general framework for understanding the  
517 response of the water cycle to global warming over land and ocean, *Hydrology and Earth System Sciences*,  
518 18, 1575-1589, 10.5194/hess-18-1575-2014, 2014.
- 519 Shuttleworth, W. J.: *Evaporation In: Maidment, DR Handbook of hydrology*, 1993.
- 520 Slatyer, R. O. and McIlroy, I. C.: *Practical microclimatology: with special reference to the water factor in*  
521 *soil-plant-atmosphere relationships*, Melbourne: Commonwealth Scientific and Industrial Research  
522 Organisation.1961.
- 523 Su, Q. and Singh, V. P.: Calibration-Free Priestley-Taylor Method for Reference Evapotranspiration  
524 Estimation, 59, e2022WR033198, <https://doi.org/10.1029/2022WR033198>, 2023.
- 525 Taoka, T., Iwata, H., Hirata, R., Takahashi, Y., Miyabara, Y., and Itoh, M.: Environmental Controls of  
526 Diffusive and Ebullitive Methane Emissions at a Subdaily Time Scale in the Littoral Zone of a Midlatitude  
527 Shallow Lake, *Journal of Geophysical Research-Biogeosciences*, 125, 10.1029/2020jg005753, 2020.

528 Thornthwaite, C. W. and Holzman, B.: Evaporation from land and water surfaces, *Monthly Weather Review*,  
529 67, 4-11, 10.1175/1520-0493(1939)67<4:doefl>2.0.co;2, 1939.

530 van Heerwaarden, C. C., de Arellano, J. V. G., Moene, A. F., and Holtslag, A. A. M.: Interactions between  
531 dry-air entrainment, surface evaporation and convective boundary-layer development, *Quarterly Journal of*  
532 *the Royal Meteorological Society*, 135, 1277-1291, 10.1002/qj.431, 2009.

533 Xiao, W., Zhang, Z., Wang, W., Zhang, M., Liu, Q., Hu, Y., Huang, W., Liu, S., and Lee, X.: Radiation  
534 Controls the Interannual Variability of Evaporation of a Subtropical Lake, *Journal of Geophysical Research-*  
535 *Atmospheres*, 125, 10.1029/2019jd031264, 2020.

536 Yang, Y. and Roderick, M. L.: Radiation, surface temperature and evaporation over wet surfaces, *Quarterly*  
537 *Journal of the Royal Meteorological Society*, 145, 1118-1129, 10.1002/qj.3481, 2019.

538 Zhao, J., Zhang, M., Xiao, W., Wang, W., Zhang, Z., Yu, Z., Xiao, Q., Cao, Z., Xu, J., Zhang, X., Liu, S.,  
539 and Lee, X.: An evaluation of the flux-gradient and the eddy covariance method to measure CH<sub>4</sub>, CO<sub>2</sub>, and  
540 H<sub>2</sub>O fluxes from small ponds, *Agricultural and Forest Meteorology*, 275, 255-264,  
541 10.1016/j.agrformet.2019.05.032, 2019.

542 Zhao, X. and Liu, Y.: Variability of Surface Heat Fluxes and Its Driving Forces at Different Time Scales  
543 Over a Large Ephemeral Lake in China, *Journal of Geophysical Research-Atmospheres*, 123, 4939-4957,  
544 10.1029/2017jd027437, 2018.

545